Energy Conversion and Management 215 (2020) 112917

Contents lists available at ScienceDirect

Energy Conversion and Management

journal homepage: www.elsevier.com/locate/enconman

Integrated approach for optimal techno-economic planning for high renewable energy-based isolated microgrid considering cost of energy storage and demand response strategies

Mark Kipngetich Kiptoo[a,*], Mohammed Elsayed Lotfy[a,b], Oludamilare Bode Adewuyi[a], Abdul Conteh[a], Abdul Motin Howlader[c], Tomonobu Senjyu[a]

[a] University of the Ryukyus, 1 Senbaru, Nishihara-cho, Nakagami, Okinawa 903-0213, Japan
[b] Zagazig University, Zagazig 44519, Egypt
[c] University of California, Riverside, CA 92521, USA

ARTICLE INFO

Keywords:
Pumped thermal energy storage (PTES)
Demand Response (DR)
Photovoltaic (PV) system
Wind turbine (WT)
Renewable generation-based dynamic pricing (RGDP) DR
System reliability

ABSTRACT

To realize an efficient energy supply system for an isolated microgrid, a joint design framework that considered the capacity sizing alongside operational planning is essential. In this work, an integrated planning model was developed to investigate the techno-economic performances of a high renewable energy-based standalone microgrid. The approach combines capacity sizing and operation scheduling, considering demand-side management strategies for different system design scenarios. The evaluated scenarios involved the combination of wind turbine, photovoltaic system, diesel generator, with either battery energy storage or pumped thermal energy storage. A demand response program based on instantaneous renewable energy availability is proposed with dynamic pricing economic model for improving the overall system flexibility. Mixed-integer linear programming algorithm on MATLAB® is deployed as the optimization solver. The minimization of the sum of system costs which includes equivalent annual costs of the investments, running costs and costs based on demand-side management strategies is the objective function. The combination of photovoltaic, wind turbine and pumped thermal energy storage is found to be the most techno-economically efficient system configuration for the considered microgrid. More so, the proposed demand response strategy minimizes the mismatch between the generation and the load demand profile effectively, thereby increasing the system flexibility.

1. Introduction

In order to meet the growing global energy deficiency and the indispensable need for universal access to reliable, clean and affordable energy by 2030, the United Nations Sustainable Development goal 7 (SDG 7) stipulates the need for an innovative transformation towards the sustainable future energy development. Hence, the massive integration and increased share of RES utilization is supported by compelling energy efficiency policies worldwide [1]; towards reducing the greenhouse gases emissions from fossil fuel sources. Microgrid technology with renewable energy resources is becoming prominently a center of research focus worldwide, especially for isolated island and places with difficult geographical terrain. An isolated microgrid can facilitate the electrification of remote islands and rural areas where the extension of the power grid is either expensive or infeasible for interconnection [2]. Microgrid also supports massive integration of the RES, ESS, as well as improve power system flexibility due to its capability to be operated in either the grid-connected or islanded mode when there is a fault in the main grid [3]. However, output of RESs are stochastic in nature which poses a greater challenge for power system operation and control upon its integration. This dictates the incorporation of expensive ESS in order to minimize the effects of intermittency in the output of the solar and wind power. Thus, without proper planning there is a high possibility that the ESS capacity can be enormously large and that can results in high cost of power system planning and operation.

1.1. Integrated planning of microgrid system considering energy storage system flexibility option

Several design criteria have been deployed in microgrid planning and operation feasibility studies in literature; some of the notable ones

* Corresponding author.
E-mail address: kiptoo.k.mark@gmail.com (M.K. Kiptoo).

https://doi.org/10.1016/j.enconman.2020.112917
Received 6 October 2019; Received in revised form 9 January 2020; Accepted 27 April 2020
Available online 11 May 2020
0196-8904/

Nomenclature

A_{wt}	blade's swept area by the wind (m^2).
I_{stc}	incident solar irradiance at standard test condition ($1kW/m^2$).
α_p	temperature coefficient of the PV module.
ΔP_L	flexible load demand (kW).
ΔP_L^{max}	maximum flexible load demand capacity (kW).
ΔP_L^{min}	minimum flexible load demand capacity (kW).
ρ	air density (kg/m^2).
BESS	Battery Energy Storage System.
C_p	power coefficient of wind turbine.
DEPF	Diesel Energy Penetration Fraction.
Dg	density of argon gas (kg/m^3).
DLCDR	Direct Load Control Demand Response.
DR	Demand Response.
DSM	Demand Side Management.
ESS	Energy Storage System.
ESS_{ptes}^{cap}	capacity of PTES (kWh).
ESS_{bess}^{cap}	capacity of BESS (kWh).
M_g	mass of argon gas (kg).
M_r	mass of PTES storage medium (kg).
P_g	instantaneous power output of diesel generator (kW).
P_L	Load demand (kW).
P_{ptes}^{ch}	charging power of PTES (kW).
P_{ptes}^{dis}	discharging power of PTES (kW).
P_{pv}	instantaneous power output of PV (kW).
P_{pv}^{cap}	capacity of PV (kW).
P_{RES}	instantaneous total RES generation (kW).
P_r^{dlc}	DLC DR electricity price (US cents/kWh).
P_r^{std}	standard electricity price (US cents/kWh).
P_r^{tou}	TOU DR electricity price (US cents/kWh).
P_{wt}	instantaneous power output of WT (kW).
P_{wt}^{cap}	capacity of WT (kW).
PTES	Pumped Thermal Energy Storage.
PV	Photovoltaics.
r	discount rate (%).
REPF	Renewable Energy Penetration Fraction.
RES	Renewable Energy Sources.
RGDPDR	Renewable Generation-based Dynamic Pricing Demand Response.
SH_g	specific heat density of argon gas (J $kg^{-1}K^{-1}$).
SH_r	specific heat density of storage medium (J $kg^{-1}K^{-1}$).
SOC^{max}	maximum state of charge of ESS (kWh).
SOC^{min}	minimum state of charge of ESS (kWh).
T	total time period in the scheduling horizon (hours).
T_{pv}	temperature of PV module.
TOUDR	Time of Use Demand Response.
Uef	volumetric efficiency of argon gas (%).
v_{ci}	cut-in wind speed.
V_{co}	cut-out wind speed.
Vs	volumetric flow rate argon gas.
WT	Wind Turbine.
Y	project lifetime (years).
Y_{pv}	derating factor of PV (%).
I_I	incident solar irradiance (W/m^2).

are levelized cost of electricity (LCOE), renewable energy fraction, loss of load probability and so on [4]. Different optimization techniques have been adopted such as the robust evolutionary algorithms [5]; a detailed comprehensive analysis of the adoption of several other meta-heuristic approaches for smart microgrid design is presented in [6]. The design of isolated microgrid takes a more peculiar approach since isolated (off-grid) microgrid cannot benefit from the flexibility provided by large grid interconnection. Hence, the flexibility management depends significantly on energy storages and the reliability condition can be fulfilled by the incorporation of standby generators. The controllability requirement of renewable energy generation has been achieved by proper integration of suitable energy storage facilities demand. A grid-connected power optimization strategy for the integration of wind power with compressed air energy storage is developed in [7]. The authors in [8] proposed a novel load control method for optimal part-load operation of compressed air energy storage system for managing generation fluctuations. The feasibility of an isolated power systems for rural electrification in northern Kenya was investigated in [9]. In reference [10], a similar configuration is investigated with the aim of ensuring a higher penetration fraction of RES towards minimizing the amount of fuel consumption based on the fuel price sensitivity analysis. In Ref. [11], a hybrid system with multiple storage facilities using BESS and pumped hydro storage, for trailing the micro- and macro-meteorological fluctuations of PV and WT energy system output, respectively is discussed.

There are diverse ESS technologies for microgrid flexibility management options in literature [12]; they are classified in terms of the investment costs, lifetime, power capacity, energy density, losses, deficiencies, *etc*. However, the problem of cost and size remains a crucial challenge to the effective deployment of ESS technologies [13]. One of the prominently recognized emerging ESS technologies is the pumped thermal energy storage system (PTES) [14]. Compared to other existing energy storage options such as BESS, compressed air energy storage and pumped-hydro energy storage, PTES has a relatively better energy density which results in reduced unit cost per MWh of capacity and per MW installation cost [15]. Also, unlike the pumped hydro energy storage system, the land area and topographical requirements are not complicated [16]. Hence, the prospects of PTES for microgrid design, especially for isolated cases, is encouraging. In this study, a detailed cost-effective and technical evaluation of PTES technology compared to BESS, with the adoption of DSM strategies is carried out. The goal is to achieve an effective microgrids configuration and capacity sizing while incorporating credible system flexibility requirements.

1.2. Prospects of demand-side management in flexibility planning of microgrid

DSM is a broad category of programs geared toward enhancement of energy efficiency in smart grids through load demand profile modifications [17]. DR program is a branch of DSM that is aimed towards motivating and influencing the electricity consumer to reshape their energy demand in response to the attractive benefits offered by the utilities [18]. The prospect of DSM and DR is enhanced by the use of advanced metering and the deregulated modern electricity market [19]. With successful deployment of DR programs, power system network expansion and additional capacity planning can be deferred [20]. This subsequently reduces the daily power system operation costs [21] and customers' electricity bills [22]. There are various types of DR proposed in the literature which are classified broadly as time-based and incentive-based DR according to motivation offered for load demand time shifting, load curtailment [23] or penalties attached for non-compliance to the bidding contract [24], and implementation strategies and applications [25]. The mathematical models for DR programs are designed to offer cost benefits to different stakeholders from the power utilities to distribution system operators, as well as, electricity consumers [26]. The time-based DR type offers time-varying electricity price to consumers while incentive-based offers fixed payments for load curtailment. The DR programs have also been devised based on consumers type; a real-time DR targeted to industrial consumers is discussed in [27] while residential consumers DR programs are extensively

addressed in [28].

1.3. Research gap and motivation for the research study

Most of the recent studies have been centered around and limited to large power systems with the benefits of network interconnection, market deregulation, diverse generation sources, and DR programs. The applicability and potential of DR programs to microgrid is still an area of growing interest, especially in terms of energy cost [29], pollution reduction [30], peak consumed load demand minimization as illustrated in reference [31], and reliability improvement [32]. Reference [33] proposed and validated the benefit of demand-side management on reducing the impact of solar and wind energy uncertainty for residential, commercial, and industrial microgrid consumers. The operation flexibility enhancement for high penetration of RESs based power systems in order to accommodate the intermittent/unpredictability of power output from wind and solar generation systems and capacity planning are still promising [34]. For a high RES generation-based isolated microgrid majorly consisting of WT and PV power generations, the operation planning flexibility depends highly on the support of limited and very expensive energy storage system for addressing the mismatch of time-varying demand and generation profiles. Thus, DSM adoption becomes an essential tool for effective and economic sizing of the system components and provision of necessary operation flexibility management for power systems with high RES penetration levels.

Moreover, the economic and technical aspect of microgrid design entails three crucial aspects that are often treated using stage-by-stage segregated approaches in many power system planning studies. These planning approaches are optimal capacity sizing, optimal energy unit scheduling, and point-to-point energy transactions [35]. These segregated planning strategies often lead to sub-optimality in the overall systems, such as under or overcapacity sizing of the system components, high operation costs, etc. This sub-optimality tends to emanate due to the long-term planning models' failure to adequately capture and validate the actual short-term operating conditions, which often tends to become more pronounced in systems with high renewable energy penetration fractions. Similarly, the short-term operation scheduling strategy studies presume that optimal system configuration is adequately predetermined, which significantly impact short-term operation planning both in terms of operation costs, power system reliability, and flexibility management requirements. Hence, this implies that the three planning models need to be unified and linked in order to realize better technical and economic benefit for the overall power system. Thus, this work proposes an integrated planning approach that combines optimal capacity sizing, operation planning, and demand-side management strategies. The three stages are simultaneously investigated and determined so as to achieve optimal configuration and operation planning strategies.

1.4. Contributions of the study

In the broad view of the existing works of literature, this study seeks to address the challenges of long-term optimum capacity and short-term operation planning for a stand-alone microgrid system consisting of wind, solar generation, and ESSs. The target is to ensure a high renewable energy penetration, using the flexibility provision capabilities of ESSs and optimal DSM strategies. Moreover, the need for an improved and adaptable DSM mechanism that addresses the challenges of variability RES that attempts to match the load demand and the RES power outputs profile is proposed. The contributions of this work are highlighted as follows:

- An integrated optimization framework that encompasses energy system components capacity sizing, operation strategies and effective DSM implementation for a high RES-based microgrid design with sufficient operation flexibility capacity is investigated.
- A relative novel renewable generation-based dynamic pricing demand response (RGDP) DR strategies that take into consideration the time-variability of RESs as a tool for effective system planning and demand-side flexibility enhancement is formulated.
- The performance of PTES that has been proven to be cost-effective and ideal ESS technology for isolated microgrids is comparatively analyzed.
- The study considered a real case study of a Kenyan microgrid that can serve as a benchmark for a sustainable pathway for future high RES-based microgrid development.

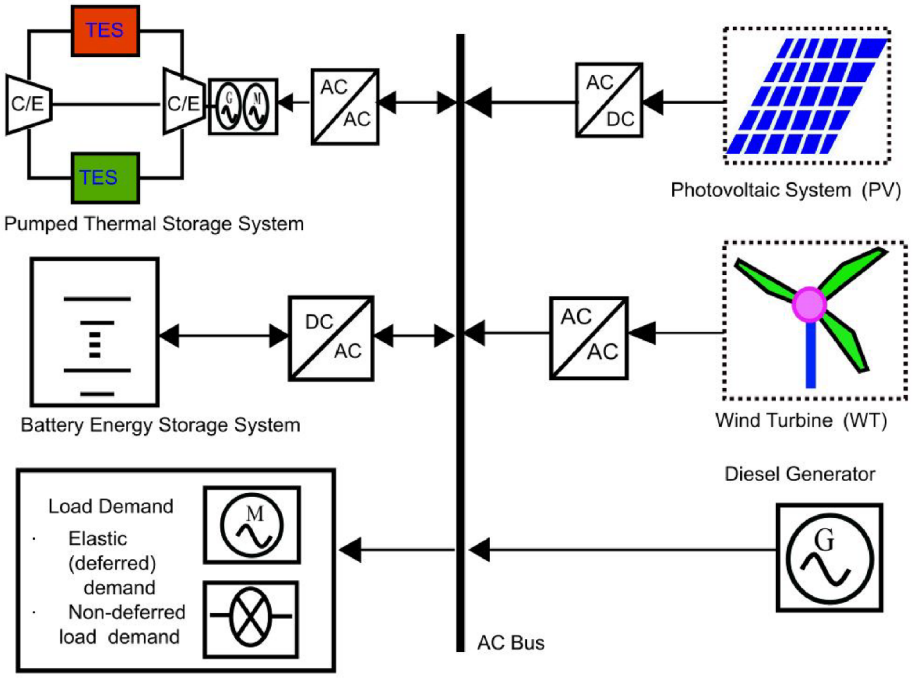

Fig. 1. Proposed system configuration.

The performance of the proposed methodology is investigated through simulations on MATLAB® environment.

2. System components description and mathematical modeling

The proposed system configuration for the discussed microgrid is as shown in Fig. 1. The proposed model comprises of the PV, WT, ESSs, and the diesel generator. Two types of ESS alternatives, namely PTES and BESS, are considered to evaluate the most techno-economically viable configuration energy supply option for the microgrid.

2.1. Wind turbine model

The total rated output power of the wind system for a specific wind turbine model can be determined using Eq. (1) [36]:

$$P_{wt}^{cap} = \left(\frac{1}{2} \times \rho \times A_{wt} \times v_r^3 \times C_p\right) \tag{1}$$

where v_r is the rated wind speed at a specified hub height and P_{wt}^{cap} is the capacity of the WT system. Hence, the total instantaneous power output of the wind system (P_{wt}), as a function of wind speed at any time t, can be estimated using the following Eq. (2):

$$P_{wt}(t) = \begin{cases} P_{wt}^{cap} \times \frac{v_r(t)^3 - v_{ci}^3}{v_r^3 - v_{co}^3} & (v_{ci} \leqslant v \leqslant v_r \\ P_{wt}^{cap} & v_r < v \leqslant v_{co} \\ 0 & v < v_{ci} \text{ and } v > v_{co} \end{cases} \tag{2}$$

2.2. PV system model

The instantaneous power output of a PV array (P_{pv}) in kW is a function of solar irradiance $I_I(t)$, temperature (T_{pv}), and temperature coefficient of the PV module (α_p). The total instantaneous power output of the PV system can be calculated using Eq. (3) as follows [37]:

$$P_{pv} = \left(P_{pv}^{cap} \times Y_{pv} \times \frac{I_I(t)}{I_{stc}} \times [1 + \alpha_p(T_{pv} - T_{stc})]\right) \tag{3}$$

where P_{pv}^{cap} is the capacity of the PV system.

2.3. Pumped thermal energy storage

The operation of PTES involves the storing of surplus power from the energy supply systems as sensible change in temperature in two separate thermal storage system [38]. PTES have been found applicable for large scale energy management applications [39], and its prospects for small-scale microgrid application in terms of cost-effectiveness and flexibility provision has been verified [40]. The operation strategy is analogous to pumped hydro energy storage (PHES) system; but rather than pumping water, heat pumping is used to create temperature difference for storing potential electrical energy in form of heat energy. PTES has the advantage of economy of scale in terms of land requirements when compared to the PHES. The theory of operation and development of PTES is adequately covered in [41]. The complete PTES system is illustrated in Fig. 2.

2.3.1. Pumped thermal energy storage operation modes

The PTES system transits between the following operational modes in cycles based on the condition of the aggregate energy system *i. e.* depending on power surplus or deficit of the energy system. The direction of charging operation is as indicated in the Fig. 2 by route 2–1-3–4. The surplus power to be stored is used to drive a heat pump equipped with compressor powered by an electric motor. The argon gas from the cold store is compressed and pumped to the hot store at +550°C, 12bars. It is then allowed to flow downwards at 0.5 m/s for maximum heat exchange, thereby transferring heat to storage material and exiting at the bottom through an expander at -160°C, 1 bar pressure. While in the cold store, it absorbs the heat from the storage material while cooling it down from initial normal room temperature. The respective temperatures for each section of the PTES are represented by T1, T2, T3 and T4 as illustrated in Fig. 2. The heat is continuously taken from the low pressure tank and delivered to the high pressure tank until the system reaches the maximum charge level [42]. In the standby mode, the PTES system is either in a fully charged or discharged state. The PTES system is discharged by reversing the operation direction *i. e.* route 1–2-4–3 as shown in Fig. 2.

2.3.2. Pumped thermal energy storage and power output dynamics

The energy stored in the PTES system per unit volume is a function of the change in the internal energies of the hot and cold medium of storage [43]. The internal energies of the mediums of storage (for both the hot h and cold c mediums) are the function of their respective mass, M_r and specific heat density, SH_r. Depending on the material used, M_r and SH_r can be the same value for both storage mediums. Thus, the energy stored can be determined by the temperature difference between the hot and cold store as described below:

$$ESS_{ptes}^{cap} = M_r^h \times SH_r^h \times (T_2(t) - T_3(t)) - M_r^c \times SH_r^c \times (T_1(t) - T_4(t)) \tag{4}$$

$$ESS_{ptes}^{cap} = M_r^h \times SH_r^h \times (T_2(t) - T_3(t) - T_1(t) + T_4(t)) \tag{5}$$

where ESS_{ptes}^{cap} is the capacity of the PTES. The power output and input P_{ptes} of the PTES per unit volume (for charging and discharging instance) is determined by the mass of gas transferred M_g, gas volumetric flow rate V_s, specific heat (SH_g), density of the gas (D_{ag}), temperature difference and volumetric efficiency (U_{ef}), which is a function of pressure and clearance ratios [15]. The charging and discharging output of PTES is simplified by Eq. (6) and (7), respectively, as described below:

$$P_{ptes}^{ch} = \epsilon_e \times M_g \times SH_g \times \{(T_2(t) - T_1(t)) - (T_3(t) - T_4(t))\} \tag{6}$$

$$P_{ptes}^{dis} = \epsilon_e \times M_g \times SH_g \times \{(T_3(t) - T_4(t)) - (T_2(t) - T_1(t))\} \tag{7}$$

where:

$$M_g = D_{ag} \times V_s \times U_{ef} \times \omega/2\Pi \tag{8}$$

ϵ_e is the conversion efficiency from thermal energy to the electrical

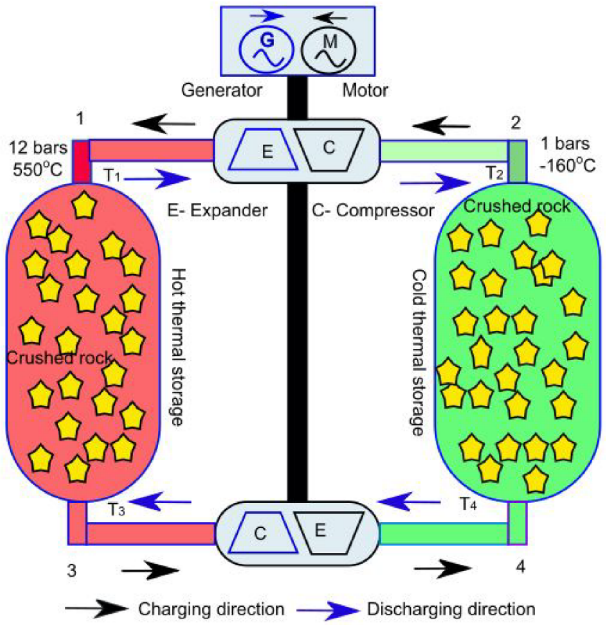

Fig. 2. Pumped thermal energy storage.

energy equivalent. The state of charge dynamic and the required capacity limits for PTES operation scheduling as a function of the optimal capacity ESS_{ptes}^{cap} are thus described:

$$SOC(t) = SOC(t-1)(1-S_{ptes}) + P_{ptes}^{ch}(t) \times \eta_{ptes}^{c} - \frac{P_{ptes}^{dis}(t)}{\eta_{ptes}^{d}} \quad (9)$$

$$SOC_{ptes}^{min} = 0.1 \times ESS_{ptes}^{cap} \quad (10)$$

$$SOC_{ptes}^{max} = 0.9 \times ESS_{ptes}^{cap} \quad (11)$$

where SOC_{ptes}^{max} and SOC_{ptes}^{min} is the maximum and minimum state of charge of the PTES, respectively. S_{ptes} is the self-discharge rate, P_{ptes}^{ch} and P_{ptes}^{dis} are the charging and discharging power to and from the PTES, η_{ptes}^{c} and η_{ptes}^{d} are the charging and discharging efficiencies of the PTES.

2.4. Battery energy storage system model

The BESS state of charge at any time t and the BESS state of charge limits as a function of optimal BESS capacity ESS_{bess}^{cap}, respectively, are given by:

$$SOC(t) = SOC(t-1)(1-S_{bess}) + P_{bess}^{ch}(t) \times \eta_{bess}^{c} - \frac{P_{bess}^{dis}(t)}{\eta_{bess}^{d}} \quad (12)$$

$$SOC_{bess}^{min} = 0.2 \times ESS_{bess}^{cap} \quad (13)$$

$$SOC_{ptes}^{max} = 0.8 \times ESS_{bess}^{cap} \quad (14)$$

where $SOC(t)$ and $SOC(t-1)$ are the current and previous energy capacity of the BESS over one time step and S_{bess} is the self-discharge rate. P_{bess}^{ch} and P_{bess}^{dis} are the charging and discharging power to and from the BESS which are functions of the energy surplus and deficits from the energy supply system, respectively. η_{bess}^{c} and η_{bess}^{d} are the charging and discharging efficiencies of the BESS.

2.5. Integrated planning framework for renewable energy-based microgrid system with demand response program consideration

Fig. 3 is the flowchart for the joint planning framework for optimal capacity sizing and operation planning with and without DR program for the system under consideration. The diesel generators serve as the standby power supply sources for the period of deficient supply from the RES and ESS; after DSM. The model also considers two types of load demands (), which are shiftable (ΔP_L) and non-shitfable loads for DSM implementation. P_{RES} is the total RES and DPSP is the deficiency of power supply probability.

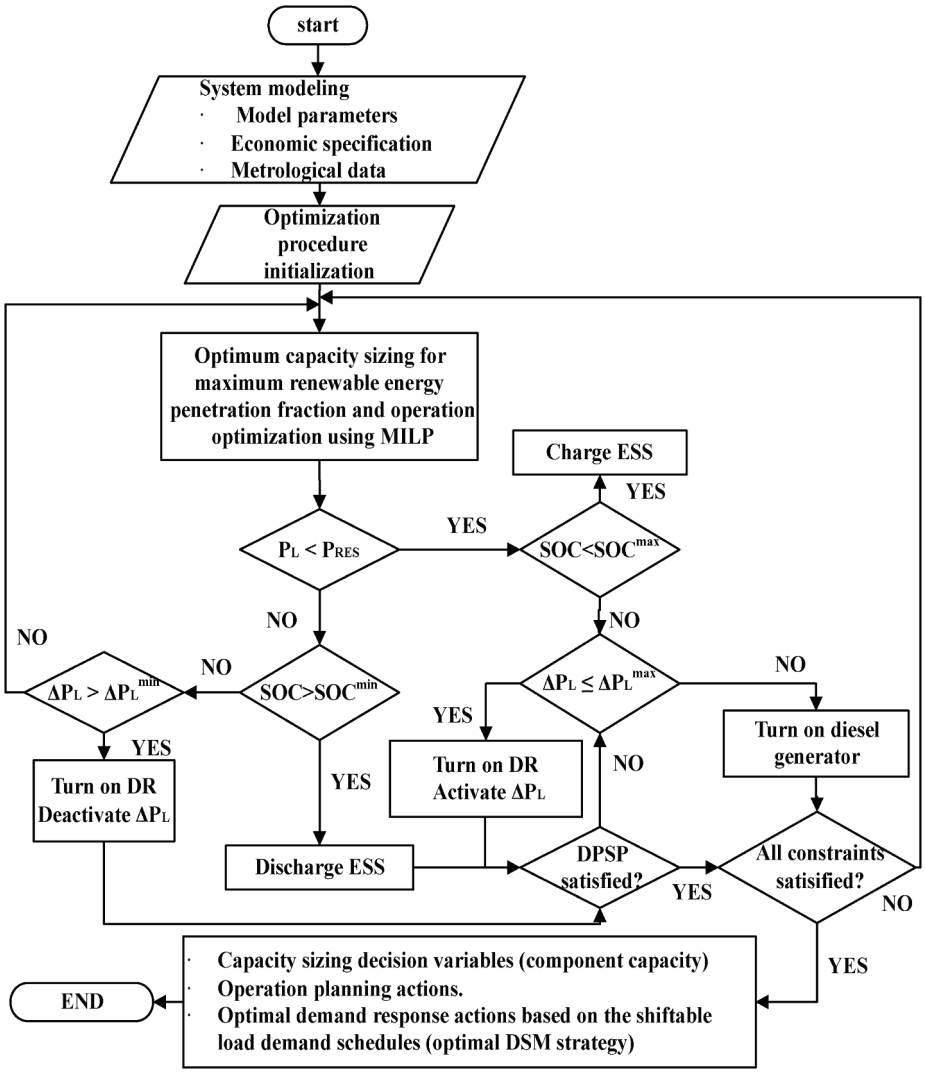

Fig. 3. The flowchart for the microgrid integrated planning framework.

3. Demand response program and economic modelling

The consumer's ability to alter their consumption patterns is directly influenced by economic factors such as the price motivation, incentive and penalty offered; and these factors depend on the type of DR adopted. The DR models consider two types of electrical appliances namely the elastic and inelastic load demand. The elastic load demand is considered to be flexible in terms of time usage, *i. e.* consumption time can be adjusted from one period to another such as the dishwashers and water pumps. The inelastic loads are the non-deferred demands that have fixed time of electricity usage. The inelastic load can be further categorized into two namely adjustable loads such as the heating and ventilation, and air conditioning (HVAC) units, and the non-adjustable loads which include the lighting loads who's states can only be on or off. An electricity price variation ($\partial P_r^{std}(i)$ or $\partial P_r^{std}(j)$) in the *i*th or *j*th single period, respectively, will result in a quantity variation of the load demand ($\partial P_L(i)$ or $\partial P_L(j)$) in the *j*th or *i*th period. Hence, the quantity of load demand for all time periods (T) is affected by the variation in electricity price for every specific *ith* or the *j*th period.

The price elasticity of load demand ($\phi_{e(i,i)}$) defines the behavioural pattern of the electrical demand to a change in its price stipulated by DR pricing scheme as defined in [44]:

$$\phi_{e(i,i)} = \frac{P_r^{std}(i)}{P_L(i)} \cdot \frac{\partial P_L(i)}{\partial P_r^{std}(i)} \; ; \quad \forall\, i, j \in T \tag{15}$$

The multi-period price sensitivity of the *i*th period versus *j*th period is given by:

$$\phi_{e(i,j)} = \frac{P_r^{std}(i)}{P_L(i)} \cdot \frac{\partial P_L(j)}{\partial P_r(j)} \; ; \quad \forall\, i, j \in T \tag{16}$$

3.1. Time-of-use demand response model

TOU DR is a time-based demand response program that offers a fixed pricing scheme for different periods of the considered cyclic time frames, such as a day or a week [26]. The TOU rate usually offers a predetermined price based on system load, such as a peak rate during hours of peak load demand (also known as peak period). The electricity cost during this period will be charged at the peak price (peak rate), this is vice versa for the periods of low loads (off-peak), where the lower possible rate (off-peak rates) is enforced. The final TOU responsive load economic model is given by:

$$P_L^{tou}(i) = P_L(i)\left\{1 + \phi_{e(i,i)}\frac{[P_r^{tou}(i) - P_r^{std}(i) + Ad(i) + Ds(i)]}{P_r^{std}(i)} + \sum_{j=1,j\neq i}^{T} \phi_{e(i,j)}\frac{[P_r^{dp}(j) - P_r^{std}(j) + Ad(j) + Ds(j)]}{P_r^{std}(j)}\right\} \; ; \quad \forall\, i, j \in T \tag{17}$$

where $P_r^{tou}(i)$ is the electricity price enforced when the TOU DR program is selected as DSM strategy, *Ad* and *Ds* are the incentives and penalties offered, respectively, for the *i*th and the jth periods.

3.2. Direct load control demand response model

DLC is a classical incentive-based DR program that offers incentives in the form of payment or electricity bill credits to the electricity consumers when they curtail their load demand; or when the power utility remotely cycles or regulate customer's electrical equipment consumption during contingencies or period of peak load demand [45]. The contractual load control technique of the DLC program has been globally adopted mainly for load reduction for residential and commercial consumers during periods of peak load demand [46]. The final responsive DLC load demand model is defined as:

$$P_L^{dlc}(i) = P_L(i)\left\{1 + \phi_{e(i,i)}\frac{[P_r^{dlc}(i) - P_r^{std}(i) + Ad(i) + Ds(i)]}{P_r^{std}(i)} + \sum_{j=1,j\neq i}^{T} \phi_{e(i,j)}\frac{[P_r^{dlc}(j) - P_r^{std}(j) + Ad(i) + Ds(j)]}{P_r^{std}(j)}\right\} \; ; \quad \forall\, i, j \in T \tag{18}$$

where $P_r^{dlc}(i)$ is the electricity price enforced when the DLC DR program is selected as DSM strategy.

3.3. Renewable generation-based dynamic pricing demand response for isolated microgrids model

The proposed RGDP is an improved time-based DR program customized for an isolated microgrid that lacks the laxity of a liberalized market. The minimization of the cost of the generation translates to the maximization of the customer's and the power utility's benefits. Thus in this program, the power utility offers flexible pricing based on the difference between the renewable energy generated and demand, and the consumers are motivated to shift their loads based on the price offered. The following are the features of RGDP model;

a. The total energy demand of the consumer before and after demand response implementation should be equal; implying that there should be no load shedding. The proportion of flexible demand resources considered are perfectly elastic.

$$\sum_{t=1}^{T} P_L^{rgdp}(t) = \sum_{t=1}^{T} P_L(t) \tag{19}$$

b. The new electricity price $P_r^{dp}(t)$ at any time t is within the maximum and minimum limit.

$$P_r^{min} \leqslant P_r^{dp}(t) \leqslant P_r^{max} \tag{20}$$

The new RGDP DR electricity price model is implemented as a function of the mismatch between the variable RES generation and customer load demand for each time period is expressed as:

$$P_r^{dp}(t) = P_r^{std}\left\{1 + \frac{P_L(t) - [P_{wt}(t) + P_{pv}(t)]}{P_L(t)}\right\} \tag{21}$$

The RGDP model determines the optimal load demand curve/profile with the application of appropriate demand response actions based on the available renewable generation that will give the minimum generation costs; thus yield minimum electricity cost for the consumer. Hence, the RGDP final load demand model is defined as:

$$P_L^{rgdp}(i) = P_L(i)\left\{1 + \phi_{e(i,i)}\frac{[P_r^{dp}(i) - P_r^{std}(i) + Ad(i) + Ds(i)]}{P_r^{std}(i)} + \sum_{j=1,j\neq i}^{T} \phi_{e(i,i)}\frac{[P_r^{dp}(i) - P_r^{std}(i) + Ad(i) + Ds(i)]}{P_r^{std}(i)}\right\} \; ; \quad \forall\, i, j \in T \tag{22}$$

4. Problem formulation using mixed-integer linear programming

The optimization problem addressed in this work is formulated as a MILP problem based on the adopted mathematical model of the system. Integrated optimal planning and operation of power system for both grid-tied [47] and standalone microgrid [48] has been solved using MILP algorithm. The robustness and tractability of MILP algorithm for modelling microgrid consisting of hybrid RES generators is verified in [49]. Hence, MILP in MATLAB® environment is adopted to solve the optimization problem considered in this work. The optimization problem is formulated as set of mixed-integer linear equations consisting of

two types of variables x; both real numbers and binary variables. The formulation of an MILP problem is presented below [50]:

$$\min f^T(x) \text{ subject to} \begin{cases} A \cdot x \leqslant b \\ Aeq \cdot x = beq \\ lb \leqslant x \leqslant ub \end{cases} \tag{23}$$

$f(x)$ is the objective function represented as a vector consisting of a linear combination of the decision variables. Matrices Aeq, and A and their corresponding vectors beq, b are the constraints modeled as inequality and equality respectively; lb and ub are the lower and upper band of the decision variables. x is the column vector of the decision variables. The MATLAB® INTLINPROG optimization toolbox is used in this study for the running the optimization procedures.

4.1. Objective function

The main objectives is to minimize the total microgrid costs which consist of the investment, replacement, maintenance and operational cost on both the long-term capacity sizing and short-term operation planning horizons considering the prospect of DSM. Hence, the aggregated objective function of the integrated framework for the microgrid design is as defined below:

$$\text{Minimize:Total microgrid costs} = f_{eac} + f_{run} + f_{dsm} \tag{24}$$

4.1.1. Equivalent annual cost of long-term capacity sizing

The first part of the objective function f_{eac} (24), is to minimize the total equivalent annual costs (EAC) which comprises of the capital costs, replacement costs (for BESS and diesel generators only), operation and maintenance costs over the project lifetime as expressed by (25) [51]. The discount rate is used to convert all the costs to their present value.

$$min: f_{eac} = \sum_{k=1}^{K} \left\{ C_k \times \left(\frac{r \times (1+r)^Y}{(1+r)^Y - 1} \right) \right\} \tag{25}$$

where Y is the lifetime of the project, r is the discount rate, C_k denotes the total discounted present cost of each system component, and subscript k denotes the system components which are PV, WT, BESS, PTES and diesel generator. C_k indicates the cost of each system component. Detailed costs component of C_k and the decision variables are elaborated as follows:

- C_{pv}: PV system costs;

$$C_{pv} = (CI_{pv} + OMC_{pv}) \times P_{pv}^{cap} \tag{26}$$

where CI_{pv} initial investment costs, OMC_{pv} is the present value of the operation and maintenance costs and P_{pv}^{cap} is the decision variable denoting the capacity of the PV system.

- C_{wt}: WT system costs;

$$C_{wt} = (CI_{wt} + OMC_{wt}) \times P_{wt}^{cap} \tag{27}$$

where CI_{wt} initial investment costs, OMC_{wt} is the present value of the operation and maintenance costs and P_{wt}^{cap} is the decision variable denoting the capacity of the WT system.

- C_{ptes}: PTES costs;

$$C_{ptes} = (CI_{ptes} + OMC_{ptes}) \times ESS_{ptes}^{cap} \tag{28}$$

where CI_{ptes} initial investment costs, OMC_{ptes} is the present value of the operation and maintenance costs and ESS_{ptes}^{cap} is the decision variable denoting the capacity of the PTES system.

- C_{bess}: BESS costs;

$$C_{bess} = (CI_{bess} + OMC_{bess} + RC_{bess}) \times ESS_{bess}^{cap} \tag{29}$$

where CI_{bess} initial investment costs, RC_{bess} and OMC_{bess} are the present value of the replacement, operation and maintenance costs, respectively, ESS_{bess}^{cap} is the decision variable denoting the capacity of the BESS system.

- C_{diesel}: diesel costs;

$$C_{diesel} = (MC_{diesel} \times H_{run} + RC_{diesel}) \tag{30}$$

where RC_{diesel} and MC_{diesel} are the present value of the replacement and maintenance costs, respectively, H_{run} denotes the number of hours which the diesel generator is running. Diesel generator is replaced after every 20,000hours of usage.

4.1.2. Hourly running costs based on scheduling of generating units

The second component of the objective function f_{run} (24), is system operation/running costs of the generating units based. The running (fuel) costs are directly proportional to the output power generated by each energy conversion technology on hourly basis; and it directly influences the optimal scheduling of diesel generators under different scenarios with different REPF.

$$f_{run} = \sum_{t=1}^{T} [(F_{diesel}(P_g(t)) \times c_f) \tag{31}$$

where $F_{diesel}(P_g(t))$ is the fuel cost function for the existing diesel generators expressed as:

$$F_{diesel} = aP_g^r + bP_g(t) \tag{32}$$

where c_f is the fuel cost (US $/L), P_g, P_g^r, a and b are the power output (kW), rated capacity (kW), fuel curve intercept coefficient (L/h/kW) and fuel curve slope (L/h/kW), respectively [52].

4.1.3. Costs based on demand-side management strategies

The third component of the objective function f_{dsm}, are the operating costs associated with controllable/flexible load demand rescheduling or curtailment based on the DSM strategy selected. The DSM-based operation costs is given by:

$$f_{dsm} = \sum_{t=1}^{T} A_d \times P_c(t) \tag{33}$$

where P_c is the curtailed load demand based on DSM strategy selected and A_d is the incentive cost value in $/kWh. The system operators compensate the end consumers for load demand curtailments through incentive payments.

4.2. System constraints

i. Power balance constraints: the total power generated by WT, PV, diesel generator and the ESS should always meet the load demand for all considered scenarios.

$$\begin{aligned} &P_{pv}(t) + P_{wt}(t) + P_{ESS}^{dis}(t) - P_{ESS}^{ch}(t) + P_g(t) \\ &\quad = P_L(t); \quad \text{without DR program} \\ &P_{pv}(t) + P_{wt}(t) + P_{ESS}^{dis}(t) - P_{ESS}^{ch}(t) \\ &\quad = P_L^{dlc}(t); \quad \text{considering DLC DR program} \\ &P_{pv}(t) + P_{wt}(t) + P_{ESS}^{dis}(t) - P_{ESS}^{ch}(t) \\ &\quad = P_L^{tou}(t); \quad \text{considering TOU DR program} \\ &P_{pv}(t) + P_{wt}(t) + P_{ESS}^{dis}(t) - P_{ESS}^{ch}(t) \\ &\quad = P_L^{rgdp}(t); \quad \text{considering RGDP DR program} \end{aligned} \tag{34}$$

where $P_{ESS}^{ch}(t)$ and $P_{ESS}^{dis}(t)$ are the instantaneous charging and discharging power from either PTES (P_{ptes}^{ch}, P_{ptes}^{dis}) or BESS (P_{bess}^{ch}, P_{bess}^{dis}) depending on the scenario.

ii. Energy storage system constraints; State of charge limit of ESS: the ESS state of charge must be within the maximum and the minimum

boundary conditions limit of the ESS as indicated in Eqs. (10), (11), (13) and (14).

$$SOC^{min} \leqslant SOC(t) \leqslant SOC^{max} \quad (35)$$

iii. Diesel generators output power constraint: the power output of the diesel generator (P_g) is bounded by the upper P_g^{max} and lower P_g^{min} generation limits.

$$P_g^{min} \leqslant P_g(t) \leqslant P_g^{max} \quad (36)$$

iv. Flexible load demand capacity constraint: the flexible load capacity ΔP_L is bounded within the maximum ΔP_L^{max} and the minimum ΔP_L^{min} allowable shift-able flexible load demand capacity (which is within the 10% of the initial load demand).

$$\Delta P_L^{min}(t) \leqslant \Delta P_L(t) \leqslant \Delta P_L^{max}(t) \quad (37)$$

v. The new electricity price: the new electricity price at any time after DR program is within the maximum P_r^{max} and minimum price limit P_r^{min}.

$$P_r^{min} \leqslant P_r^{dp} \leqslant P_r^{max} \quad (38)$$

5. Case study and simulation evaluation criteria

The proposed approach is implemented on a Kenyan microgrid for the Marsabit county, which is a small isolated power system. The site is currently served by two identical diesel generators Perkins model MPG-1000kVA-PK@50 Hz with rated real power of 800 kW each at 0.8 power factor on standby mode. The meteorological data (for 2.3369°N, 37.9904°E) were obtained from [53,54], economic and technical specifications of the components [55] and hourly load demand are all site-specific, and based on Kenyan economic situation as summarized in Table 1.

5.1. Simulation scenarios

In this study, transition pathways towards energy sustainability from conventional generation (diesel) towards high renewable energy penetration fraction considering the prospect of DSM is investigated using different simulation scenarios. The simulation results of different ESS technology were also compared to illustrate the cost-benefit of PTES inclusion in place of BESS. Hence, nine optimization scenarios were carried out using multiple system configurations, as explained below:

- Scenario 1: Existing system (base case); diesel generators only (REPF = 0%, DEPF = 100%).
- Scenario 2: Hybrid system configuration; PV, WT, PTES with diesel generator (REPF = 25% and DEPF = 75%).
- Scenario 3: Hybrid system configuration; PV, WT, PTES with diesel generator (REPF = 50% and DEPF = 50%).
- Scenario 4: Hybrid system configuration; PV, WT, PTES with diesel generator (REPF = 75% and DEPF = 25%).
- Scenario 5: High renewable energy-based microgrid configuration (REPF = 100%); PV, WT with PTES without DR program.
- Scenario 6: High renewable energy-based microgrid configuration (REPF = 100%); PV, WT with BESS without DR program.
- Scenario 7: High renewable energy-based microgrid configuration (REPF = 100%); PV, WT with PTES considering DLC DR.
- Scenario 8: High renewable energy-based microgrid configuration (REPF = 100%); PV, WT with PTES considering TOU DR.
- Scenario 9: High renewable energy-based microgrid configuration (REPF = 100%); PV, WT with PTES considering RGDP DR.

For the implementation of the DR programs for scenario 7, 8 and 9, the maximum elastic load demand subject to DR is taken to be 10% of load demand at each time period. The choice of 10% was based on reported analysis in existing literature [62]. The operational and cost parameters of the system components are as summarized in Table 1. The unit capacity of PV and WT is taken to be 1 kW and 50 kW respectively. The operating lifetime of the diesel generator was considered as 20,000 h. The site is currently served by two identical diesel generators; thus, the investment costs for diesel generators which is for future replacements and maintenance costs were approximated to be 1521 US $/kW and 0.012 US $/h, respectively [58]. All the future costs: replacements and maintenance costs considered during the project lifetime are discounted back to their present value using a discount rate. 0.0161 L/h/kW and 0.2486 L/h/kW are considered to be the intercept and the slope of the fuel curve, respectively, for the diesel generator considered in this study [63]. The existing diesel generators in the system are treated as backup to meet the energy deficit during the period of less generation from the RES. Hence, they are changing with the variation in load demand and the renewable energy sources power output. This can be achieved by the automatic governor control of modern generators; the same concept has been adopted in [64].

The proposed PTES design adopted in our work utilized the expertise, economic and technical specification introduced in [57] for the Kenyan case deployment and it has a prototypical capacity of up to 16 MWh [42]. In this study, the lithium-ion (nickel cobalt aluminum oxide (NCA)) BESS type was selected in order to ascertain the techno-

Table 1
Technical, cost and lifetime parameters of the system components.

Technical and economic parameters		
Economics [55]		
Discount rate	4%	
System lifetime Y	20	Years
Fuel Price c_f	1	US $/l
Photovoltaic (PV) system [56]		
Investment Cost	1695	US $/kW
Operation and maintenance cost	26	US $/kW/yr
(PV) derating factor	0.88	
lifetime	20	years
Pumped thermal energy storage (PTES) [57]		
Round trip efficiency	70%	
Investment cost (Power capacity based)	406	US $/kW
Investment cost (Energy capacity based)	15.08	US $/kWh
Operation and maintenance cost (Power capacity based)	12.76	US $/kW/yr
Operation and maintenance cost (Energy capacity based)	0.03	US $/kWh/yr
Hourly self-discharge	0.04%	
Lifetime	20	years
Wind turbine [55]		
Investment cost	2030	US $/kW
Operation and maintenance cost	76	US $/kW/yr
lifetime	20	years
Cut-in wind speed:	4	m/s
Rated wind speed:	14.5	m/s
Cut-out wind speed:	25	m/s
Survival wind speed:	60	m/s
Wind Shear Coefficient	0.143	
Diesel generators [58]		
Lifetime (operating hours)	20,000	hours
Rated Power	2 × 800 (2 units)	kW
Replacement costs	1521	US $/kW
Operating and maintenance costs	0.012	US $/hour
Lithium-ion battery energy storage system (nickel cobalt aluminum oxide (NCA))		
Investment cost [59]	330	US $/kWh
Replacement cost	330	US $/kWh
Round trip efficiency [60]	90%	
lifetime [61]	10	years

economic advantage of the proposed PTES technology. Key superior advantages of Lithium-ion batteries relative to other ESS technologies include high round trip efficiency, low self-discharge rate, high energy, and power density, long lifetime, thus requires fewer replacements over the project lifetime, etc. [12]. Moreover, lithium-NCA BESS type has comparatively high energy density with relatively lower cost relative to other lithium ESS variants in the market [59]. Thus, in this work, lithium NCA battery type was the most suitable ESS technology for comparison with PTES.

5.2. System reliability and set-up for varying renewable energy penetration assessment and analysis

System reliability analysis are considered to evaluate and ensure desired performances are guaranteed [65]. The considered system reliability index and energy supply source fraction are as listed below:

- Deficiency of power supply probability (DPSP): DPSP is expressed as the ratio of the sum of all load demand curtailments (LDC) to the total load demand during the considered period.

$$DPSP = \frac{\sum_{t=1}^{T} LDC(t))}{\sum_{t=1}^{T} P_L(t)} \tag{39}$$

- Renewable energy penetration fraction (REPF): various intermediate injection levels of REPF are evaluated in this study to illustrate transition pathways towards high RES generation-based microgrid design. The REPF is the fraction of the energy supplied by the RES to the total load demand as the RES fraction is gradually increased towards high renewable energy penetration.

$$REPF = \left(\frac{\sum_{t=1}^{T} P_{wt}(t) + P_{pv}(t) + P_{ptes}^{dis}(t) - P_{ptes}^{ch}(t)}{\sum_{t=1}^{T} P_L(t)} \right) \times 100\% \tag{40}$$

- Diesel energy penetration fraction (DEPF): DEPF represents the diesel power fraction used to satisfy the remaining net-load demand after introducing the RES and ESS at various REPF to meet the acceptable reliability.

$$DEPF = \left(1 - \frac{\sum_{t=1}^{T} P_{wt}(t) + P_{pv}(t) + P_{ptes}^{dis}(t) - P_{ptes}^{ch}(t)}{\sum_{t=1}^{T} P_L(t)} \right) \times 100\% \tag{41}$$

5.3. Electricity cost and tariffs structure

The current electricity prices and tariff structures are derived based on the Kenyan Energy Regulatory Commission (ERC) tariff settings [66]. The type of electricity consumers considered in this scope is the residential consumers as categorized in [67]. According to the current Kenyan electricity tariff structure, the flat electricity price for residential customers, which is 15.80 US cents per kWh, is taken as the standard electricity price P_r^{std} in this study. The maximum peak price and the minimum off-peak price are taken as 20.00 US cents per kWh and 10.00 US cents per kWh, respectively under the Kenyan tariff structure [68]. Scenario 9 adopts dynamic pricing scheme with the maximum and minimum price limits taken as 20.00 US cents per kWh and 10.00 US cents per kWh, respectively. The implementation of Scenario 8, considering TOU DR program, divides the load profile into three different pricing periods namely shoulder rates (1.00 am to 7.00 am), off-peak rates (7.00 am to 7.00 pm) and peak rates (7.00 pm to 1.00 am). Scenario 7 adopts the standard pricing scheme of with an incentive payment to consumers as compensation for any load curtailment (50% of the P_r^{std}). Table 2 shows the self and multi-period price elasticity of the load demand for the DRP programs pricing scheme [26]:

Table 2
DR program self and multi-period price elasticity.

	Shoulder-peak	Off-peak	Peak
Shoulder-peak	−0.1	0.01	0.012
Off-peak	0.01	−0.1	0.016
Peak	0.012	0.016	−0.1

6. Simulation results and discussions

The simulation results and discussions of the nine investigated scenarios are presented as follows;

(i.) **Scenario 1: Existing system (base case); diesel generators only (REPF = 0%, DEPF = 100%).**
This scenario is the base case, which is a representative of the current real system in place; the microgrid is evaluated based on the existing diesel generators only. The total EAC for the PV-WT-ESS is 0.00 $/year since there is no inclusion of PV, WT and ESS in this scenario. The total EAC for maintenance and replacement of the diesel generators over the project lifetime is 6.60 × $10^5$$/year with a total running cost of 2.77 × $10^{6"}$"/year. Thus the total microgrid cost is 3.43× $10^6$$/year, which is very expensive and environmentally unfriendly. The optimal scheduling of the diesel generators on short-term planning horizon is illustrated in Fig. 4. The simulation results for the optimum sizing and operation planning of the microgrid is summarized in Table 3.

(ii.) **Scenario 2: Hybrid system configuration; PV, WT, diesel generator with PTES (REPF = 25% and DEPF = 75%).**
In this case, a REPF of 25% with a 75% DEPF system design is considered for optimum capacity sizing and operation planning optimization. The simulation results of the suggested optimal system configuration are as summarized in Table 3. The simulation result shows that an injection of 240 kW of PV, 565 kW of WT and 1200 kW of PTES with a total EAC of 1.45× $10^5$$/year for WT-PV-PTES and 5.65× $10^5$$/year for diesel generators resulted in a cost-saving of 26.46% of the total running costs compared to the base case. As illustrated in Fig. 5, a combination of the WT-PV-PTES with the net-load demand being served by diesel generators, was able to meet the load demand requirement. This optimum system configuration resulted in a cost-saving of about 19.9% of the total microgrid costs compared to the base case. The operation feasibility, state of charge, charging and discharging dynamics of the ESS (PTES) is illustrated in Fig. 5 and Fig. 6, respectively.

(iii.) **Scenario 3: Hybrid system configuration; PV, WT, PTES with diesel generator (REPF = 50% and DEPF = 50%).**
In this case, a hybrid microgrid configuration of 50% RES penetration with the incorporation of ESS and diesel generator was considered, which is 25% increase in REPF as compared to scenario 2. The total EAC for WT, PV and PTES is 2.91× $10^5$$/year and for the diesel generator is 4.74× $10^5$$/year with optimal capacities of 481 kW, 1129 kW and 2400 kWh for PV, WT and PTES, respectively. The details of the simulation results are summarized in Table 3. The optimal planning result shows a notable reduction in the total running costs of about 52.57% compared with the base case (Scenario 1). Overall, the obtained optimal system configuration resulted in a significant reduction of about 39.40% of the total costs of about 39.40% compared to the base case (Scenario 1). The operation feasibility, state of charge, charging and discharging dynamics of the ESS (PTES) is

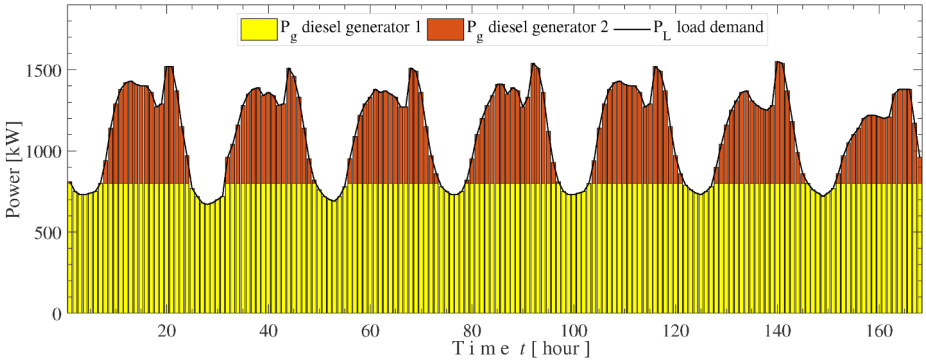

Fig. 4. Operation feasibility for REPF = 0% & DEPF = 100% system configuration consisting of diesel generation only (Scenario 1).

Table 3
Comparison of components size and costs for scenarios 1 to 4 microgrid configurations.

Configuration	Scenario 1	Scenario 2	Scenario 3	Scenario 4
REPF	0%	25%	50%	75%
DEPF	100%	75%	50%	25%
Capacity of PV (P_{pv}^{cap}) kW	0	240	481	717
Capacity of WT (P_{wt}^{cap}) kW	0	565	1129	1696
Capacity of PTES (ESS_{ptes}^{cap}) kWh	0	1200	2400	3600
Total running costs for diesel (US $/year)	2.77×10^6	2.03×10^6	1.31×10^6	6.00×10^5
EAC for diesel generators (US $/year)	6.60×10^5	5.65×10^5	4.74×10^5	3.96×10^5
Total EAC for PV, WT and PTES (US $/year)	0.00	1.45×10^5	2.91×10^5	4.36×10^5
Total microgrid costs (US $/year)	3.43×10^6	2.74×10^6	2.08×10^6	1.43×10^6

illustrated in Fig. 7 and Fig. 8, respectively.

(iv.) **Scenario 4: Hybrid system configuration; PV, WT, PTES with diesel generator (REPF = 75% and DEPF = 25%).**
This case represents a REPF of 75%, and it yielded optimal capacities of 717 kW, 1696 kW and 3600kWh for PV, WT and PTES, respectively. The transition from scenario 3 to 4 resulted in remarkable running costs reduction of about 78.30%, which is the highest as compared to the former scenarios (from 1 to 3). The decline in the running cost, as mentioned earlier, is as a result of the significant reduction of the DEPF of the microgrid's power mix. However, it's worth noting that the above transitions result in a steady increase in the total EAC for the PV, WT and ESS. The overall system configuration resulted in a reduction of about 58.2% of the total EAC compared to the base case. The costs and capacities comparisons are as summarized in Table 3. The operation feasibility, state of charge, charging and discharging dynamics of the ESS (PTES) is illustrated in Fig. 9 and Fig. 10 respectively.

(v.) **Scenario 5: High renewable energy-based microgrid configuration (REPF = 100%); PV, WT with PTES without DR program.**
This scenario considers a high renewable energy penetration fraction (REPF = 100%) with the inclusion of PTES without demand response. This scenario is the reference case for 100% REPF. The operation feasibility and energy generation profiles for the system is as shown by Fig. 11. Fig. 12 shows the mismatch between power generation and the load demand profiles. In this system, the treatment of uncertainty of the RES is crucial since there exists no dispatchability or controllability of the generation sources. Hence, this dictates the incorporation of ESS for energy management, levelling the fluctuating load demand and smoothing the stochastic output of the RES generation. This is the reason for such an enormous capacity of the PTES (ESS_{ptes}^{cap}) of 7800kWh which is the largest compared to the previous scenarios. Fig. 13 depicts the state of charge, charging and discharging dynamics of the PTES. The PTES charges and discharges during periods of surplus and deficit generation, respectively, to offset the mismatch between the generation and load demand profiles. The optimum capacities of the PV, ESS and WT are as summarized in Table 4.

(vi.) **Scenario 6: High renewable energy-based microgrid configuration (REPF = 100%); PV, WT with BESS without DR program.**
Table 4 summarizes the costs and components size comparison for PTES and BESS-based microgrid configurations without demand response program considerations for DPSP values equal to 0%, 5% and 10%. As illustrated in Table 4, the use of the PTES is shown to be more economical energy storage system alternative compared to BESS. The total microgrid cost for a PTES-based configuration is 6.44×10^5 $/year while that of a BESS-based

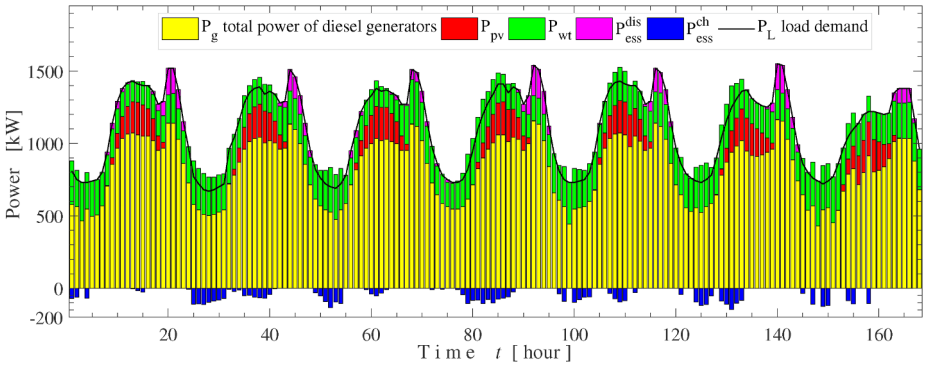

Fig. 5. Operation feasibility for the hybrid system configuration; REPF = 25% and DEPF = 75% (Scenario 2).

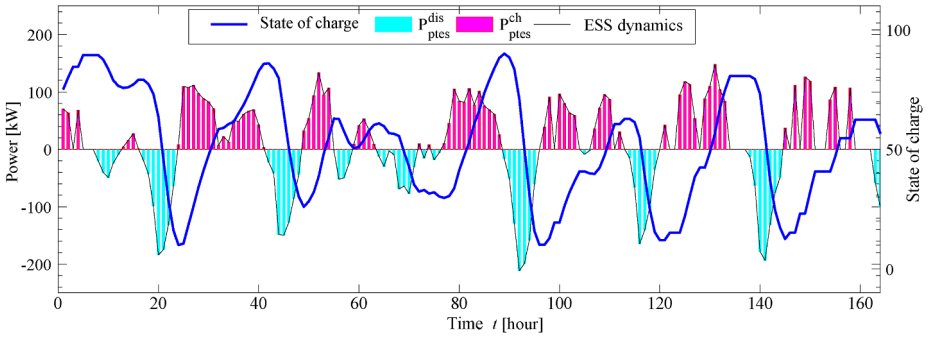

Fig. 6. State of charge, charging and discharging dynamics of the ESS for hybrid configuration (Scenario 2).

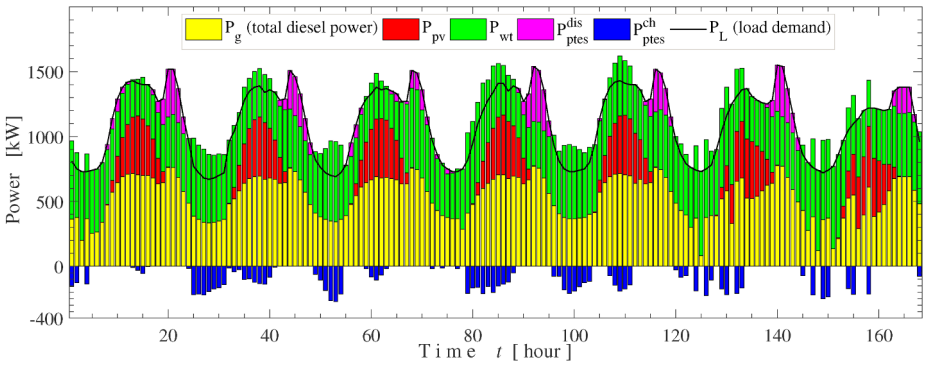

Fig. 7. Operation feasibility for hybrid configuration; REPF = 50% and DEPF = 50% generation with inclusion of ESS (Scenario 3).

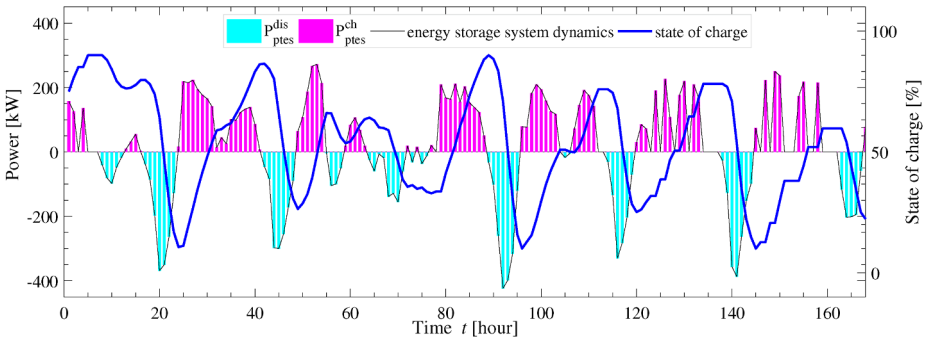

Fig. 8. State of charge, charging and discharging dynamics of the ESS for the hybrid configuration (Scenario 3).

system is 3.25×10^6 $/year at DPSP value equal to zero. The total microgrid costs of a PTES-based system is just a 1/5 of the BESS-based system. This implies adopting a PTES-based microgrid configuration will yield a significant cost saving of about 80.12% of the total cost as compared to the BESS-based microgrid. Thus the results mentioned above justify our selection of the ESS alternative for our microgrid deployment. The cost-benefit of adopting the PTES-based over BESS-based microgrid system is attributed to the potential of PTES to achieve a higher depth of discharge compared to the BESS. This capacity reduction trend is

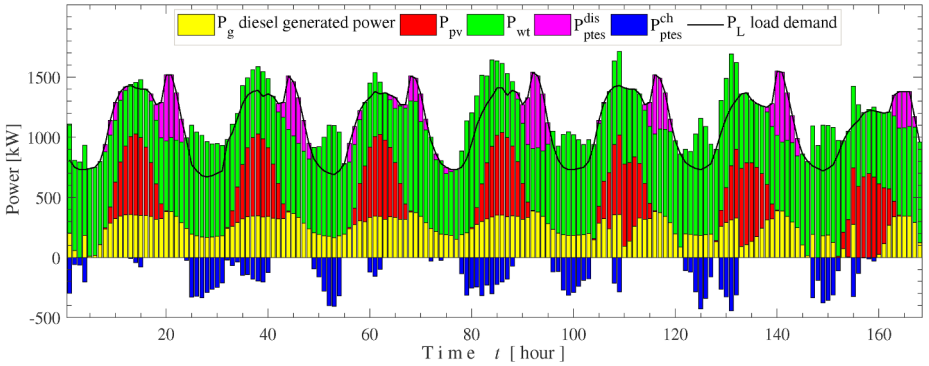

Fig. 9. Operation feasibility for hybrid configuration RES and diesel generator generation with inclusion of ESS (scenario 4).

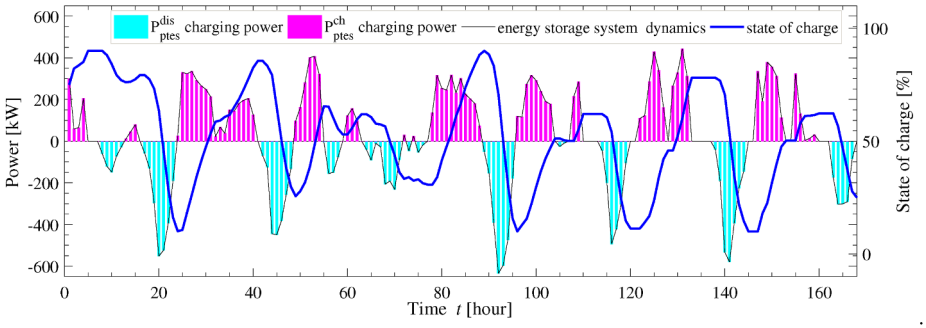

Fig. 10. State of charge, charging and discharging dynamics of the ESS for the hybrid configuration (scenario 4).

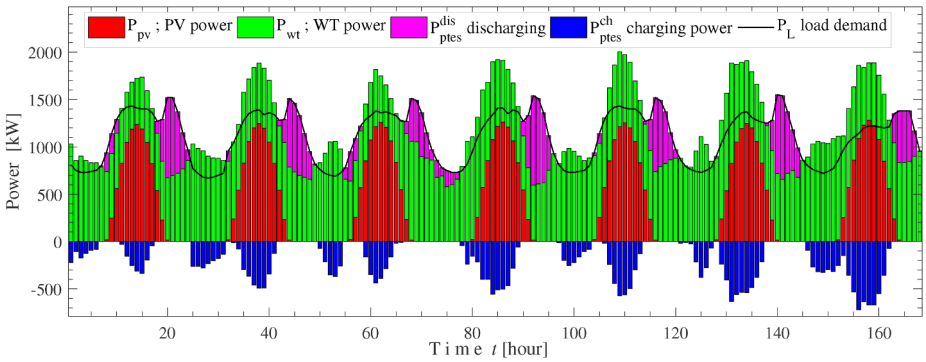

Fig. 11. Operation feasibility for 100% REPF with PTES (Scenario 5).

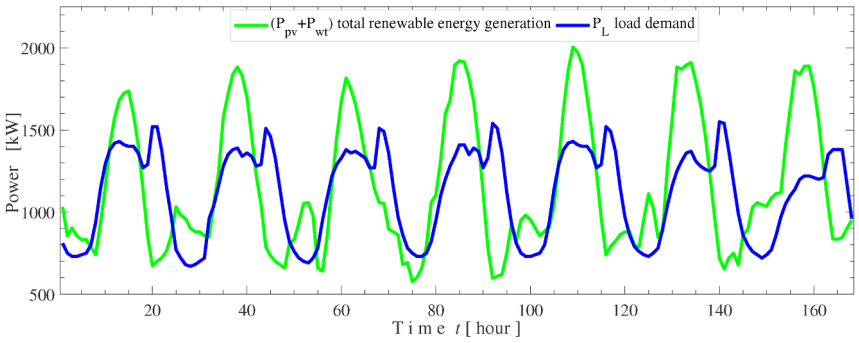

Fig. 12. Mismatch between the total RES generation and load profile (scenario 5).

also noted in microgrid configurations with 5% and 10% DPSP reliability index.

(vii.) **Scenario 7: High renewable energy-based microgrid configuration (REPF = 100%); PV, WT with PTES considering DLC DR.**

Fig. 14 shows the initial and the final economic load demand profile after DLC DR program incorporation. In this scenario, the outcome of the DLC DR is the most undesired among the considered DR programs since it penalizes all the parties involved in order to achieve feasibility of operation. From the demand side,

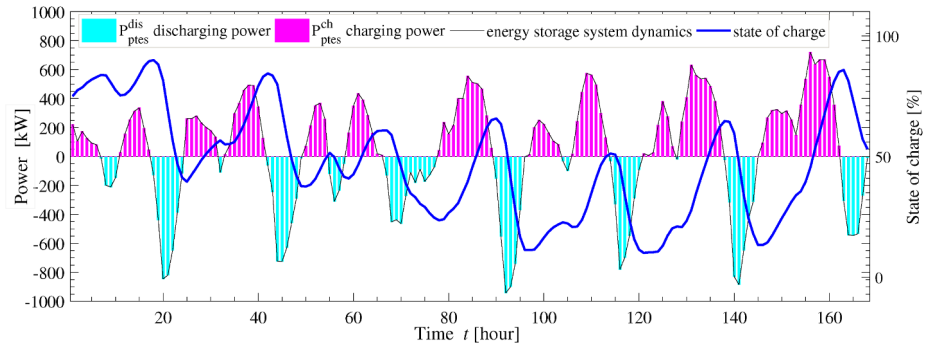

Fig. 13. State of charge, charging and discharging dynamics of the ESS for REPF = 100% system (Scenario 5).

Table 4
Costs and components size comparison for PTES and BESS-based microgrid configurations without demand response program considerations.

Configuration Microgrid type	Scenario 5:REPF = 100% PTES-based system			Scenario 6: REPF = 100% BESS-based system		
DPSP	**0%**	**5%**	**10%**	**0%**	**5%**	**10%**
Capacity of PV (P_{pv}^{cap} kW)	1316	1117	998	1267	1250	1164
Capacity of WT (P_{wt}^{cap} kW)	1928	1951	1914	1898	1797	1735
Capacity of ESS (kWh)	7800	6000	4800	9000	7200	6000
Total microgrid costs (US $/year)	6.44×10^5	5.80×10^5	5.31×10^5	3.25×10^6	2.67×10^6	2.27×10^6

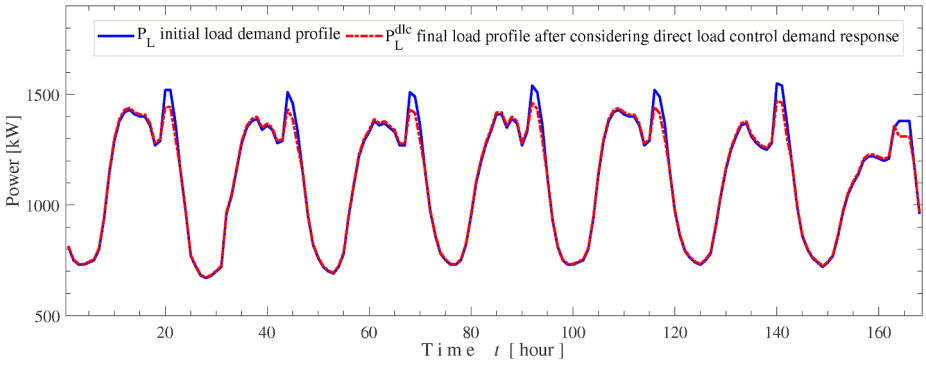

Fig. 14. DLC DR load profile.

the consumers experience an LDC of about 0.28% through load shedding. Similarly, the utility experiences revenue loss in terms of incentive payments. The electricity customers participating in this program will receive compensation for load curtailment of about 2.18×10^3 $/year. Simulation results are as summarized in Table 5. Overall, the incorporation of the DLC DR into optimal planning resulted in a 0.32% cost-saving in the total microgrid cost compared to the reference case (scenario 5).

(viii.) **Scenario 8: High renewable energy-based microgrid configuration (REPF = 100%); PV, WT with PTES considering TOU DR**. The final economic TOU load demand profile when the electricity consumers embrace the TOU varying electricity rates per periods is as shown in Fig. 15. It is worth noting that the new load profile provides a reduction in component capacities of WT and PTES by 3.73% and 7.69% respectively. However, there is an increase of about 7.90% in the PV capacity size. Overall, it can be inferred that the resulting system configuration offers a mutual cost benefit to the utility and the consumers as depicted in Table 5. The consumer gain through a decrease in expenditure on electricity by 5.95% while the power utility achieves a decrease of 2.47% of the total microgrid costs compared to the base case (scenario 5) as illustrated in Table 6. When consumers adjust

Table 5
Demand-Side cost-benefit comparison for the three DR programs.

Configuration DR type	scenario 5 without DR	scenario 7 DLC DR	scenario 8 TOU DR	scenario 9 RGDP DR
Customer bill (US $/year)	1,544,361.52	1,540,032.00	1,452,464.00	1,421,108.00
% change customer bill	-	−0.28%	−5.95%	−7.98%
DR incentive costs (US $/year)	0.00	2.18×10^3	0.00	0.00
Energy consumed (kWh)	9,774,440	9746880	9,768,200	9,774,440
% change in energy consumed	–	−0.28%	−0.06%	0%

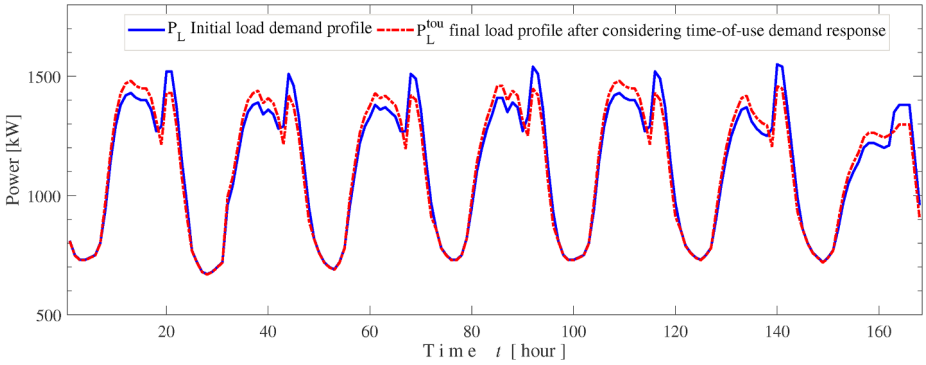

Fig. 15. TOU DR load profile.

Table 6
Configuration and total microgrid cost comparison for three DR programs.

Configuration DR type	scenario 5 –	scenario 7 DLC DR	scenario 8 TOU DR	scenario 9 RGDP DR
Capacity of PV (P_{pv}^{cap} kW)	1316	1387	1420	1399
% change in P_{pv}^{cap}	–	5.40%	7.90%	6.31%
Capacity of WT (P_{wt}^{cap} kW)	1928	1869	1856	1848
% change in P_{wt}^{cap}	–	−3.06%	−3.73%	−4.11%
Capacity of PTES (ESS_{ptes}^{cap} kWh)	7800	7800	7200	6600
% change in ESS_{ptes}^{cap}	-	0	−7.69%	−15.38%
DR incentive costs (US $/year)	0.00	2.18×10^3	0.00	0.00
Total microgrid costs (US $/year)	6.44×10^5	6.45×10^5	6.29×10^5	5.93×10^5
% change in total microgrid costs	–	0.02%	−2.47%	−7.97%

their load demand to achieve minimum electricity cost, the system efficiency is significantly improved. This improvement of system efficiency is as a result of the load demands being shifted from peak rate to the off-peak rate pricing periods. Thereby, the cost of generation by the power utility and the electricity customers bill are consequentially reduced. However, it can also be noted that this program also leads to a decrease in the total load demand of about 0.06%. This decrease in load demand implies that the electricity consumer will undergo some load reduction, which is undesired. The incorporation of the TOU DR into capacity planning resulted in a 2.47% cost-saving in the total microgrid costs compared to the reference case (scenario 5).

(xi.) **Scenario 9: High renewable energy-based microgrid configuration (REPF = 100%); PV, WT with PTES considering RGDP DR**.

In this scenario, the RGDP DR strategies are formulated such that the difference between the available RES generation and the load demand is minimized. Thus, a dynamic pricing scheme based on the mismatch between the load demand and the generation profiles is adopted. The new electricity price after the implementation of the RGDP DR program is illustrated in Fig. 16. The application of RGDP DR has a significant benefit to all the aspect of planning framework. From the demand side, the electricity consumers enjoy the highest cost-saving of about 7.98% for the same amount of energy consumed compared to the reference case which is without a DR program (scenario 5). Moreover, the RGDP DR offers the cheapest total electricity bill for the consumers compared to the DLC and TOU DR program as shown in Table 5. Moreover, the total energy consumed is equal to the initial energy demand in reference case (scenario 5) implying that the DR does not interfere with the customer's load demand and that their demand is fully satisfied at all time which makes it more superior than DLC and TOU DR. The demand-side cost-saving is derived from the fact that the consumers have shifted their load from high electricity price periods to the low price periods.

From the generation-side, the implementation of the RGDP DR program results in 15.38% and 4.11% reduction in WT and PTES capacities, respectively, compared to the reference case (Scenario 5) which is without the DR program. This is the highest percentage reduction in value compared to the DLC and TOU DR types in Table 6. The resultant 7.97% reduction in EAC for each component and the overall total costs of the microgrid system is a consequence of the benefit of the WT, and PTES capacity reduction for the new system configuration. Also, while the system decreased the capacity of WT, it increased the capacity of PV by 6.31%. This due to the fact that EAC of the PV is relatively cheaper compared to WT.

The reason behind the success of the RGDP DR program, worth noting, is that by offering flexible, dynamic pricing as a function of the differences between the generated power and the load demand, as shown in Fig. 16; the consumers are motivated to shift their load demand from high electricity price periods to low price periods as a result of the new pricing scheme; thereby yielding a new optimal load profile. The new optimal RGDP load profile obtained is much cheaper in terms of microgrid planning costs for the utility thus offers the minimum electricity costs for the end consumer compared to the reference case (scenario 5). From Fig. 17, it is observed that the RGDP DR tends to drive the peak load demand to match the peak period of renewable energy generation profile. By minimizing the difference between the instantaneous generation and the corresponding load demand, the capacity of the ESS (PTES) is also significantly minimized by 15.38%.

7. Conclusions

An integrated optimal planning framework for a high renewable energy-based microgrid for off-grid energy supply considering ESS and renewable generation-based dynamic pricing demand response has been discussed. This work was designed to validate different prospects of combined long-term capacity sizing planning, operation optimization, as well as demand-side flexibility management towards achieving a techno-economically efficient energy system. The optimal demand-side management strategy ensured that the system is flexible on a short-term basis by minimizing the mismatch between the generation and load profile thereby guaranteeing the minimization of the total microgrid cost for system development as well as electricity cost for the consumers. A step by step REPF values allows the validation of the transition path towards 100% green energy-based system design. From the simulation results, PV-WT-PTES is found to be the most techno-economically efficient system configuration for the considered

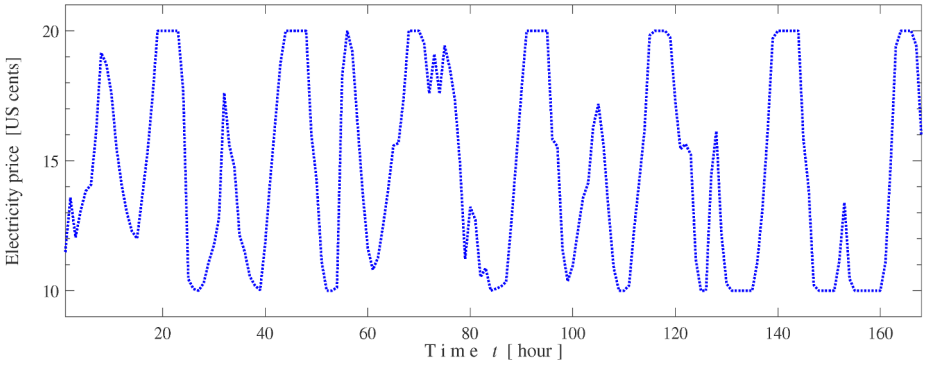

Fig. 16. The new electricity price in US cents after implementation of RGDP DR program.

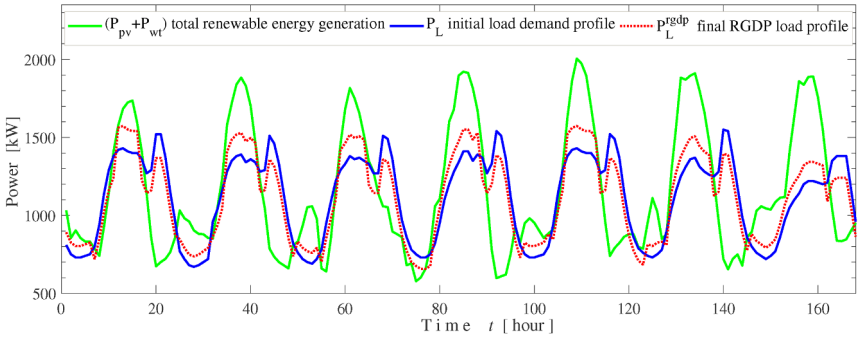

Fig. 17. The new RGDP DR load profile after implementation of the RGDP DR program.

microgrid. The inclusion of PTES is shown to be more economical compared to BESS in the optimum microgrid configuration. The total microgrid cost of PTES-based system is about one-fifth of the BESS-based system, resulting in a significant cost saving of about 80.12% in the total cost in comparison to the BESS-based microgrid. The RGDP DR strategies for effective capacity optimization are formulated such that the difference between the available RES generation and the load demand is minimized. Thus, the implementation of the proposed RGDP DR has shown to be more advantageous compared to conventional TOU DR and DLC DR programs. The resultant system using RGDP DR program showed a significant reduction of the total microgrid cost by 7.97%, which is the highest compared to DLC and TOU DR programs. Therefore, the proposed framework serves as a general benchmark and a platform for optimal planning for sustainable RES-based microgrid development.

CRediT authorship contribution statement

Mark Kipngetich Kiptoo: Conceptualization, Data curation, Formal analysis, Investigation, Methodology, Resources, Software,Validation, Visualization, Writing - original draft, Writing - review & editing. **Mohammed Elsayed Lotfy:** Formal analysis and Validation, Writing - review & editing. **Oludamilare Bode Adewuyi:** Formal analysis and Validation, Writing - review & editing. **Abdul Conteh:** Validation and Visualization. **Abdul Motin Howlader:** Validation. **Tomonobu Senjyu:** Supervision.

Declaration of Competing Interest

The authors declare that they have no known competing financial interests or personal relationships that could have appeared to influence the work reported in this paper.

Acknowledgments

The authors wish to acknowledge the Japan international cooperation agency (JICA) for the support provided in the form of African business education (ABE) scholarship to the main author (M. K. Kiptoo) towards the success of this research work. The authors also wish to appreciate the effort of Mr.Hannington Gochi of REA, Kenya office for supplying the principal data needed for this project.

References

[1] Lee JT, Callaway DS. The cost of reliability in decentralized solar power systems in sub-Saharan Africa. Nature Energy 2018;3:960.
[2] Domenech B, Ranaboldo M, Ferrer-Martí L, Pastor R, Flynn D. Local and regional microgrid models to optimise the design of isolated electrification projects. Renewable Energy 2018;119:795–808.
[3] Sufyan M, Rahim NA, Tan C, Muhammad MA, Raihan SRS. Optimal sizing and energy scheduling of isolated microgrid considering the battery lifetime degradation. PloS one 2019;14.
[4] Kolhe M, Ranaweera KIU, Gunawardana AS. Techno-economic optimum sizing of hybrid renewable energy system. IECON 2013–39th Annual Conference of the IEEE Industrial Electronics Society IEEE; 2013. p. 1898–903.
[5] Zhang G, Wu B, Maleki A, Zhang W. Simulated annealing-chaotic search algorithm based optimization of reverse osmosis hybrid desalination system driven by wind and solar energies. Solar Energy 2018;173:964–75. https://doi.org/10.1016/j.solener.2018.07.094.
[6] Khan B, Singh P. Selecting a meta-heuristic technique for smart micro-grid optimization problem: A comprehensive analysis. IEEE Access 2017;5:13951–77. https://doi.org/10.1109/ACCESS.2017.2728683.
[7] Tong S, Cheng Z, Cong F, Tong Z, Zhang Y. Developing a grid-connected power optimization strategy for the integration of wind power with low-temperature adiabatic compressed air energy storage. Renewable Energy 2018;125:73–86.
[8] Cheng Z, Tong S, Tong Z. Bi-directional nozzle control of multistage radial-inflow turbine for optimal part-load operation of compressed air energy storage. Energy Conver Manage 2019;181:485–500.
[9] Lukuyu JM, Cardell JB. Hybrid power system options for off-grid rural electrification in northern kenya. Smart Grid Renewable Energy 2014;5:89.
[10] Aziz AS, Tajuddin MFN, Adzman MR, Ramli MA, Mekhilef S. Energy management and optimization of a pv/diesel/battery hybrid energy system using a combined dispatch strategy. Sustainability 2019;11:683.
[11] Adewuyi OB, Komolafe OA. Optimal operational analysis of off-grid hybrid renewable energy system with multiple storage facilities. Int J Sci Eng Res 2016;7:379–90.
[12] IRENA (2017), Electricity storage and renewables: Costs and markets to 2030, 2017.
[13] Adewuyi OB, Shigenobu R, Ooya K, Senjyu T, Howlader AM. Static voltage stability improvement with battery energy storage considering optimal control of active and reactive power injection. Electric Power Syst Res 2019;172:303–12. https://doi.org/10.1016/j.epsr.2019.04.004.
[14] Klumpp F. Comparison of pumped hydro, hydrogen storage and compressed air energy storage for integrating high shares of renewable energies–potential, cost-comparison and ranking. J Energy Storage 2016;8:119–28. https://doi.org/10.1016/j.est.2016.09.012.
[15] McTigue JD, White AJ, Markides CN. Parametric studies and optimisation of pumped thermal electricity storage. Appl Energy 2015;137:800–11.
[16] Benato A. Performance and cost evaluation of an innovative pumped thermal electricity storage power system. Energy 2017;138:419–36. https://doi.org/10.1016/j.energy.2017.07.066.
[17] Aghaei J, Alizadeh M-I. Demand response in smart electricity grids equipped with renewable energy sources: a review,. Renewable Sustainable Energy Rev 2013;18:64–72. https://doi.org/10.1016/j.rser.2012.09.019.
[18] Albadi MH, El-Saadany EF. Demand response in electricity markets: An overview. 2007 IEEE Power Engineering Society General Meeting 2007. p. 1–5. https://doi.org/10.1109/PES.2007.385728.
[19] Zhang Q, Li J. Demand response in electricity markets: a review. 2012 9th International Conference on the European Energy Market IEEE; 2012. p. 1–8.
[20] Kiptoo MK, Adewuyi OB, Lotfy ME, Ibrahimi A, Senjyu T. Harnessing demand-side management benefit towards achieving a 100% renewable energy microgrid. Energy Reports 2020;6(2):680–5. https://doi.org/10.1016/j.egyr.2019.11.137.
[21] Nikoukar J. Unit commitment considering the emergency demand response programs and interruptible/curtailable loads. Turkish J Electr Eng Computer Sci 2018;26:1069–80.
[22] Jin M, Feng W, Marnay C, Spanos C. Microgrid to enable optimal distributed energy retail and end-user demand response. Appl Energy 2018;210:1321–35. https://doi.org/10.1016/j.apenergy.2017.05.103.
[23] Shigenobu R, Adewuyi OB, Yona A, Senjyu T. Demand response strategy management with active and reactive power incentive in the smart grid: A two-level optimization approach. AIMS Energy 2017;5:482–505. https://doi.org/10.3934/energy.2017.3.482.
[24] Moghaddam MP, Abdollahi A, Rashidinejad M. Flexible demand response programs modeling in competitive electricity markets. Appl Energy 2011;88:3257–69. https://doi.org/10.1016/j.apenergy.2011.02.039.
[25] Vardakas JS, Zorba N, Verikoukis CV. A survey on demand response programs in smart grids: Pricing methods and optimization algorithms. IEEE Commun Surveys Tutorials 2015;17:152–78. https://doi.org/10.1109/COMST.2014.2341586.

[26] Aalami H, Moghaddam MP, Yousefi G. Modeling and prioritizing demand response programs in power markets. Electric Power Syst Res 2010;80:426–35.
[27] Olawuyi N, Akorede M, Femi E, Ayeni A, Jimoh R. Real-time demand response algorithm for minimising industrial consumers electricity billing. 2017 IEEE 3rd International Conference on Electro-Technology for National Development (NIGERCON) IEEE; 2017. p. 1061–6.
[28] Wang Z, Paranjape R, Sadanand A, Chen Z. Residential demand response: An overview of recent simulation and modeling applications. 2013 26th IEEE Canadian Conference on Electrical and Computer Engineering (CCECE) IEEE; 2013. p. 1–6.
[29] Yan X, Ozturk Y, Hu Z, Song Y. A review on price-driven residential demand response. Renewable Sustainable Energy Rev 2018;96:411–9.
[30] Tabar VS, Ghassemzadeh S, Tohidi S. Energy management in hybrid microgrid with considering multiple power market and real time demand response. Energy 2019;174:10–23.
[31] Amrollahi MH, Bathaee SMT. Techno-economic optimization of hybrid photovoltaic/wind generation together with energy storage system in a stand-alone micro-grid subjected to demand response. Appl Energy 2017;202:66–77. https://doi.org/10.1016/j.apenergy.2017.05.116.
[32] Khalili T, Jafari A, Abapour M, Mohammadi-Ivatloo B. Optimal battery technology selection and incentive-based demand response program utilization for reliability improvement of an insular microgrid. Energy 2019;169:92–104.
[33] Aghajani G, Shayanfar H, Shayeghi H. Demand side management in a smart micro-grid in the presence of renewable generation and demand response. Energy 2017;126:622–37. https://doi.org/10.1016/j.energy.2017.03.051.
[34] Dranka GG, Ferreira P. Review and assessment of the different categories of demand response potentials. Energy 2019;179:280–94.
[35] Kiptoo MK, Adewuyi OB, Lotfy ME, Amara T, Konneh KV, Senjyu T. Assessing the techno-economic benefits of flexible demand resources scheduling for renewable energy–based smart microgrid planning. Future Internet 2019;11:219.
[36] Shariatzadeh F, Mandal P, Srivastava AK. Demand response for sustainable energy systems: a review, application and implementation strategy. Renewable Sustainable Energy Rev 2015;45:343–50.
[37] Kharrich M, Akherraz M, Sayouti Y. Optimal sizing and cost of a microgrid based in pv, wind and bess for a school of engineering. 2017 International Conference on Wireless Technologies, Embedded and Intelligent Systems (WITS) IEEE; 2017. p. 1–5.
[38] Howes J. Concept and development of a pumped heat electricity storage device. Proc IEEE 2012;100:493–503.
[39] Desrues T, Ruer J, Marty P, Fourmigué J. A thermal energy storage process for large scale electric applications. Appl Thermal Eng 2010;30:425–32.
[40] Vandersickela A, Aboueldahabb A, Spliethoffc H. Small-scale pumped heat electricity storage for decentralised combined heat and power generation: cost optimal design and operation. Proceedings of ecos 2016-the 29th international conference on efficiency, cost, optimization, simulation and environmental impact of energy systems june 19–23, 2016, portorož, slovenia. 2016.
[41] Pumped heat electrical storage (phes), 2019. URL:http://energystorage.org/energy-storage/technologies/pumped-heat-electrical-storage-phes.
[42] Smallbone A, Jülch V, Wardle R, Roskilly AP. Levelised cost of storage for pumped heat energy storage in comparison with other energy storage technologies. Energy Conver Manage 2017;152:221–8.
[43] White A, Parks G, Markides CN. Thermodynamic analysis of pumped thermal electricity storage. Appl Thermal Eng 2013;53:291–8.
[44] Yousefi S, Moghaddam MP, Majd VJ. Optimal real time pricing in an agent-based retail market using a comprehensive demand response model. Energy 2011;36:5716–27.
[45] Chen C, Wang J, Kishore S. A distributed direct load control approach for large-scale residential demand response. IEEE Trans Power Syst 2014;29:2219–28.
[46] A. Salami, M.M. Farsi, Demand side management using direct load control for residential and industrial areas, in: 2015 International Congress on Electric Industry Automation (ICEIA 2015), 2015, pp. 11–16. doi10.1109/ICEIA.2015.7165839.
[47] Chen J, Zhang W, Li J, Zhang W, Liu Y, Zhao B, Zhang Y. Optimal sizing for grid-tied microgrids with consideration of joint optimization of planning and operation. IEEE Trans Sustainable Energy 2018;9:237–48. https://doi.org/10.1109/TSTE.2017.2724583.
[48] Atia R, Yamada N. Sizing and analysis of renewable energy and battery systems in residential microgrids. IEEE Trans Smart Grid 2016;7:1204–13. https://doi.org/10.1109/TSG.2016.2519541.
[49] Mashayekh S, Stadler M, Cardoso G, Heleno M. A mixed integer linear programming approach for optimal der portfolio, sizing, and placement in multi-energy microgrids. Appl Energy 2017;187:154–68. https://doi.org/10.1016/j.apenergy.2016.11.020.
[50] Luna AC, Diaz NL, Graells M, Vasquez JC, Guerrero JM. Mixed-integer-linear-programming-based energy management system for hybrid pv-wind-battery microgrids: Modeling, design, and experimental verification. IEEE Trans Power Electron 2017;32:2769–83. https://doi.org/10.1109/TPEL.2016.2581021.
[51] Hemmati R, Saboori H, Siano P. Coordinated short-term scheduling and long-term expansion planning in microgrids incorporating renewable energy resources and energy storage systems. Energy 2017;134:699–708.
[52] Askarzadeh A. Distribution generation by photovoltaic and diesel generator systems: Energy management and size optimization by a new approach for a stand-alone application. Energy 2017;122:542–51. https://doi.org/10.1016/j.energy.2017.01.105.
[53] Weather mount marsabit, 2019. URL:https://www.meteoblue.com/en/weather/forecast/week/mount-marsabit_kenya_187584/.
[54] Photovoltaic geographical information system., 2019. URL:https://rem.jrc.ec.europa.eu.
[55] The Presidency, Republic of Kenya, Power generation and transmission master plan, kenya medium term plan 2015–2020 - vol. i, 2016. URL:https://www.erc.go.ke/.
[56] Ministry of Energy and Petroleum, Republic of Kenya, Updated least cost power development plan 2017–2037, 2018. URL:http://www.decoalonize.org/wp-content/uploads/2019/09/LCPDP-Least-Cost-Power-Development-Plan-2017-2037-not-2022-updated-June-2018.pdf.
[57] Kiptoo MK, Adewuyi OB, Lotfy ME, Senjyu T, Mandal P, Abdel-Akher M. Multi-objective optimal capacity planning for 100% renewable energy-based microgrid incorporating cost of demand-side flexibility management. Appl Sci 2019;9:3855.
[58] Rehman S, Alam MM, Meyer J, Al-Hadhrami LM. Feasibility study of a wind-pv-diesel hybrid power system for a village. Renewable Energy 2012;38:258–68. https://doi.org/10.1016/j.renene.2011.06.028.
[59] Kairies KP. Battery storage technology improvements and cost reductions to 2030: a deep dive. Int Renew Energy Agency Work 2017;2017.
[60] Jaiswal A. Lithium-ion battery based renewable energy solution for off-grid electricity: a techno-economic analysis. Renewable Sustainable Energy Rev 2017;72:922–34.
[61] Dhundhara S, Verma YP, Williams A. Techno-economic analysis of the lithium-ion and lead-acid battery in microgrid systems. Energy Conver Manage 2018;177:122–42.
[62] Aalami H, Moghaddam MP, Yousefi G. Demand response modeling considering interruptible/curtailable loads and capacity market programs. Appl Energy 2010;87:243–50.
[63] Rahman MM, Khan MM-U-H, Ullah MA, Zhang X, Kumar A. A hybrid renewable energy system for a north american off-grid community. Energy 2016;97:151–60. https://doi.org/10.1016/j.energy.2015.12.105.
[64] Moradi H, Esfahanian M, Abtahi A, Zilouchian A. Optimization and energy management of a standalone hybrid microgrid in the presence of battery storage system. Energy 2018;147:226–38. https://doi.org/10.1016/j.energy.2018.01.016. URL:http://www.sciencedirect.com/science/article/pii/S0360544218300161.
[65] Dong W, Li Y, Xiang J. Optimal sizing of a stand-alone hybrid power system based on battery/hydrogen with an improved ant colony optimization. Energies 2016;9:785.
[66] Tarrif setting: Electricity., 2019. URL:https://www.erc.go.ke/services/economic-regulation/tarrif-setting/tarrif-setting-electricity/.
[67] Electricity cost tariffs & schedule of tariffs 2018, 2019. URL:http://kplc.co.ke/content/item/691/electricity-cost-tariffs—schedule-of-tariffs-2018.
[68] Electricity cost in kenya., 2019. URL:https://stima.regulusweb.com/.